Influence of contact geometry on the magnetoresistance of elliptical rings

D. Morecroft,[a] F. J. Castaño, W. Jung, J. Feuchtwanger, and C. A. Ross[b]
Department of Materials Science and Engineering, Massachusetts Institute of Technology, Cambridge, Massachusetts 02139

(Received 16 November 2005; accepted 11 March 2006; published online 27 April 2006)

Room temperature magnetotransport measurements have been carried out on NiFe single layer and NiFe/Cu/Co/Au multilayer elliptical rings. The shape of the magnetoresistance response is strongly dependent on the contact configuration and the direction of the applied field with respect to the easy axis of the ellipse. The magnetization states and magnetoresistance can be quantitatively modeled. © *2006 American Institute of Physics*. [DOI: 10.1063/1.2199470]

Ferromagnetic ring-shaped structures with mesoscopic lateral dimensions show a range of stable magnetic states that could be useful in magnetoelectronic applications for storing and manipulating information.[1–3] Recently, there has been a great deal of interest in electrical transport measurements of small circular magnetic rings.[4–11] This technique allows characterization of individual rings, and it is the most likely candidate for a practical application. To date, low temperature[4–8] and room temperature[9–11] transport measurements have been carried out on single-layer circular rings, and the results show that the transitions between the bidomain "onion" and the flux-closure "vortex" states can be identified by a characteristic change in the anisotropic magnetoresistance (AMR). Most of the reported magnetotransport measurements on rings use a two-point electrical configuration and Saitoh *et al.*[7] used symmetrical four-point measurements in a "Wheatstone-bridge" arrangement. The influence of the electrical contact geometry on the magnetoresistance (MR) has not been considered. This letter describes how the contact geometry influences the measured MR in NiFe single-layer and NiFe/Cu/Co/Au multilayer elliptical rings. An elliptical geometry is chosen to introduce shape anisotropy and control the locations of domain walls.[12]

The samples consisted of 28 nm thick single-layer elliptical NiFe rings with a 4 μm major axis, aspect ratio (major/minor axis) of 2, and widths from 200 to 300 nm, and NiFe (4 nm)/Cu (5 nm)/Co (7 nm)/Au (4 nm) pseudo spin valve (PSV) elliptical rings with a 1.9 μm major axis, aspect ratio of 2, and widths of 80 nm and above. Four nonmagnetic contact wires were fabricated using lift-off processing, and a multilevel lithography process that included electron-beam (e-beam) and optical lithographies for pattern generation, and ultrahigh vacuum sputtering or e-beam evaporation for the metallization steps.[13] Room temperature MR measurements were carried out using a four-point probe technique with a constant rms current of 5 μA at a frequency of 1 kHz, with ac lock-in detection.

We first consider the NiFe single-layer ring shown in Fig. 1(a). The inset is an electrical circuit model of the ring, which shows that the total current is divided into I_1 and I_2, the ratio of which is the inverse of the ratio of the resistances R_1 and R_2, where $R_2=R_A+R_B+R_C$. The change in resistivity due to AMR depends on the angle θ between the current and the magnetization direction, defined as

$$\rho = \rho_\perp + (\rho_\parallel - \rho_\perp)\cos^2\theta, \tag{1}$$

where $\rho_\parallel$ and $\rho_\perp$ are the resistivities for $\theta=0°$ and $\theta=90°$, respectively. The measured resistance in Fig. 1(a) is

$$V_{12}/I = (R_1 R_B)/(R_1 + R_2). \tag{2}$$

This shows that the resistance is sensitive to changes in magnetization occurring at any position within the ring.

The MR of the unpatterned NiFe film, defined as $[(R-R_{min})/R_{min}\times 100\%]$ was 1.1%, and the resistivity values were $\rho_\parallel=21.47\ \mu\Omega$ cm and $\rho_\perp=21.24\ \mu\Omega$ cm. Figure 1(b) shows that the measured MR of the ring has maxima of 0.46% and 0.22%, for applied fields along the major and minor axes. When the field is applied along the major axis, two clear steps can be seen at ±70 and ±360 Oe, while the minor axis direction shows a gradual increase in MR as the field is reduced from positive saturation, and then a decrease when the field is increased in the negative direction. Distinct and reproducible dips in the minor axis measurement, labeled with the letter "A," occur around ±340 Oe.

In order to interpret the measurements, two-dimensional micromagnetic simulations were carried out using the NIST object oriented micromagnetic framework (OOMMF),[14] with standard parameters for NiFe, a cell size of 10 nm, and a damping coefficient $\alpha=0.5$. The resistance of each section (R_1, R_A, R_B, and R_C) of the modeled ellipse was then calculated by appropriately summing the contributions of $\cos^2\theta$ from each of the cells, and the net resistance of the elliptical ring was calculated from Eq. (2). Figure 1(c) shows the simulated MR measurements (half the loops are shown for clarity). The data are in close agreement with the experimental measurements both in terms of the switching fields and the absolute values of MR. For both the major and minor axis simulations, the gradual increase in MR as the field is decreased from saturation is due to the magnetization relaxing to align parallel to the edges of the ring. For the major axis measurement the formation of domain walls in the onion state at the ends of the elliptical ring reduces the MR close to zero field. The steps in MR at ±70 and ±360 Oe represent the formation and annihilation of the vortex state, respectively. The vortex state represents a maximum AMR, because the magnetization and the current are parallel all around the ellipse.

When the applied field is along the minor axis, there is no domain wall formed in section R_B, between the voltage

[a]Electronic mail: dm267@mit.edu
[b]Author to whom correspondence should be addressed; electronic mail: caross@mit.edu

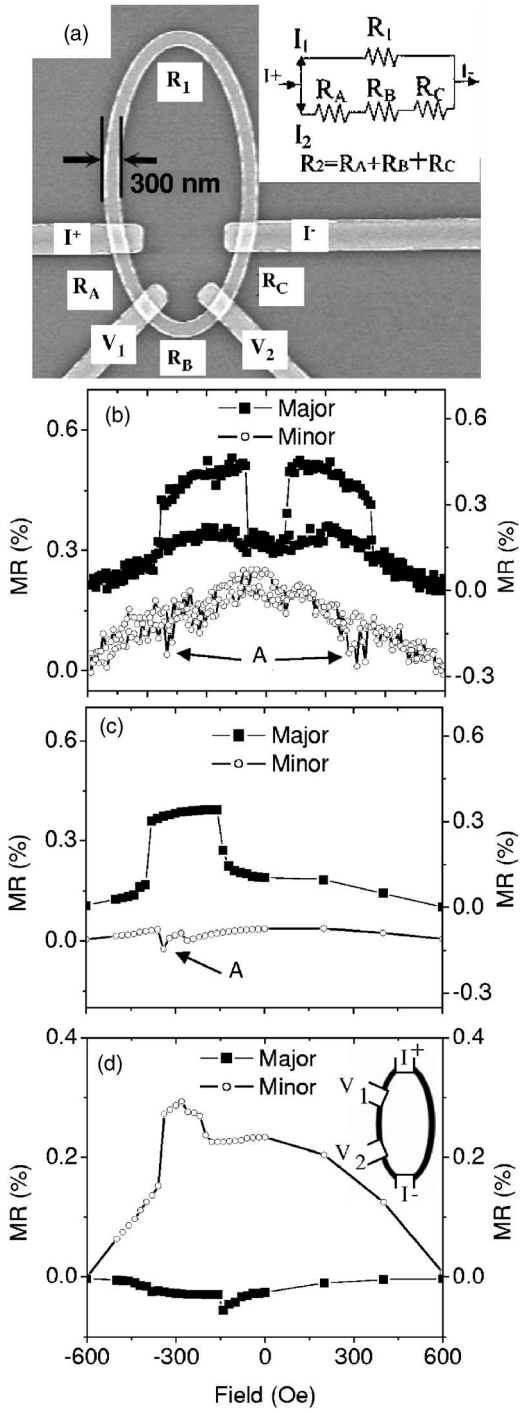

FIG. 1. (a) Scanning electron micrograph (SEM) of a single-layer 300 nm wide NiFe elliptical-ring device. The micrograph shows the current and voltage leads (I^+, I^-, V_1, and V_2) and the labels for the resistance of individual parts of the ring (R_1, R_A, R_B, and R_C). The inset shows an electrical circuit model of the ellipse, where $R_2=R_A+R_B+R_C$. (b) Corresponding MR measurements for applied field directions along the major and minor axes of the ellipse. Corresponding vertical axis for each measurement starts at 0%. The letter "A" identifies two distinct and reproducible dips in the minor axis measurements at ±340 Oe. (c) Simulated magnetotransport measurements when the field is applied along the major and the minor axes, respectively. (d) Simulated MR measurements for fields applied along the major and the minor axes and corresponding to a different contact configuration.

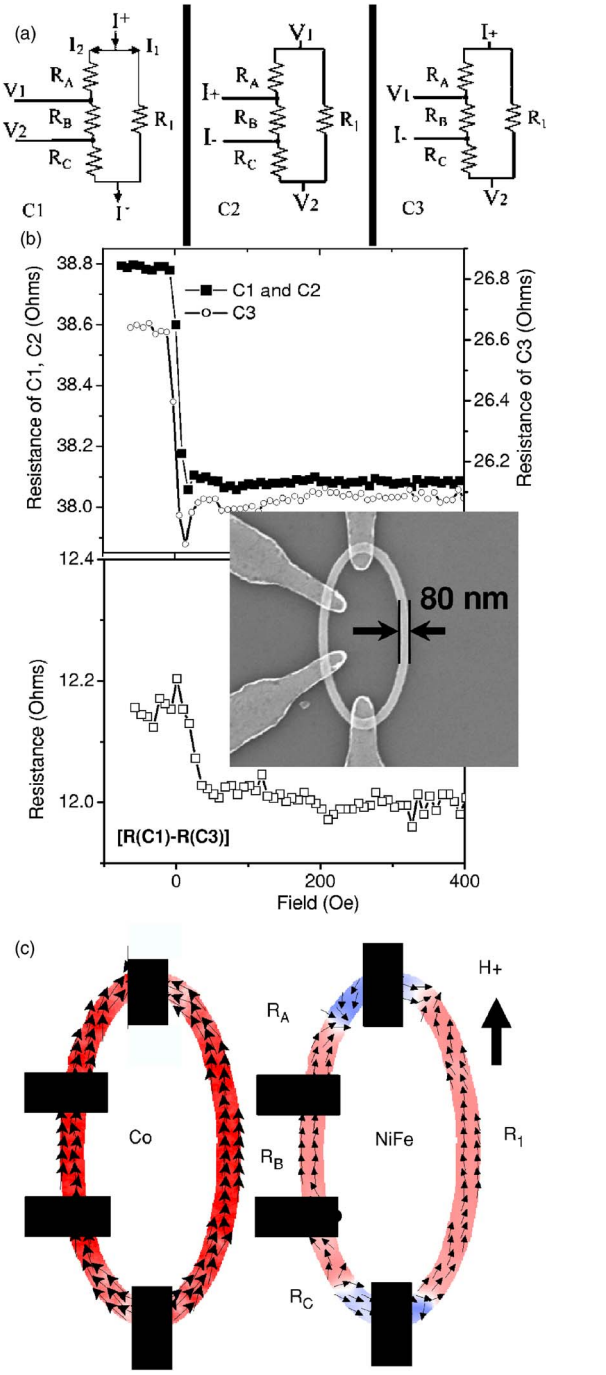

FIG. 2. (Color online) (a) Circuit diagrams for three different contact configurations labeled C1, C2, and C3 tested on a 80 nm wide NiFe/Cu/Co PSV elliptical ring. For each circuit $R_1=R_A+R_B+R_C$, and $R_A=R_B=R_C$. (b) Measured resistance vs applied field for the contact configurations C1, C2, C3, and (C1–C3). The arrows indicate the y axis for each plot. The inset shows a corresponding SEM of the PSV ring devices. (c) Micromagnetic simulations of the Co and NiFe layers in the PSV ellipse at remanence after saturation in the H^+ field direction. The figure also shows the resistance regions R_A, R_B, R_C, and R_1 around the ellipse.

contacts. A vortex state is formed, but the vortex exists over a narrower field range than in the case of a field along the major axis direction.[12] It is interesting to note that the simulations predict the dip along the minor axis, as observed in the experimental data [see Fig. 1(c)]. The simulations indicate that this is due to a spatial variation of the magnetization direction, which has been reported in NiFe thin film circular rings.[6]

For comparison, the MR of the same elliptical ring was then calculated based on a different contact configuration in which the current enters and leaves at the ends of the elliptical ring and the voltage contacts are along one arm of the ellipse [Fig. 1(d)]. Since the same micromagnetic simulations were used for both Figs. 1(c) and 1(d), the results show

the effects of contact configuration only. For the second configuration there is only a small change in MR when the field is applied along the major axis, but a larger MR for a minor axis field, in contrast to the results of Fig. 1(c), a result of the locations of the domain walls with respect to the voltage contacts.

We now consider the influence of contact configuration on the giant magnetoresistance of a NiFe/Cu/Co/Au PSV elliptical ring. This differs from the AMR of the NiFe ring because the giant magnetoresistance (GMR) of the multilayer depends on the angle between the magnetization directions of the Co and NiFe layers and not on the angle between the current and the magnetization. Figure 2 shows the three different contact configurations tested. For the first configuration C1, the voltage contacts were positioned on one side of the ellipse, for C2 they were at the ends, and for C3 one voltage contact was on the side and the other at the end of the ellipse. For C1 and C2 the measured resistance is given by Eq. (2), but for C3 the measured resistance is

$$\frac{V_{12}}{I} = \frac{(R_1 R_B) - (R_A R_C)}{R_1 + R_2}, \tag{3}$$

which differs from Eq. (2) by a term $(-R_A R_C)$ in the numerator. In the absence of GMR, taking $R_1/3 = R_A = R_B = R_C$ due to the symmetry of the contact placement, the expected resistance is $R_B/2$ for C1 and C2, and $R_B/3$ for C3.

Micromagnetic simulations of the multilayer ring were carried out using three-dimensional OOMMF (cell size =5 nm, α=0.5). Figure 2(c) shows the magnetization in the Co and NiFe layers at remanence after saturating in the positive field direction (denoted H^+). The NiFe layer reverses by the propagation of reverse domains from the ends of the ellipse. At remanence the ends of the NiFe ring have started to reverse [sections R_A and R_C in Fig. 2(c)]. As reversal proceeds, the NiFe ring forms a reverse onion state containing 360° walls, described as a twisted onion state.[13] This reversal mechanism is a result of the magnetostatic interaction from the domain walls in the Co layer, and differs from the behavior of single-layer NiFe rings.

Experimentally, the ring was initially saturated in a major axis field, and then swept from +400 Oe and to –100 Oe, so that the NiFe layer changed between a forward onion and a reverse twisted onion state, while the Co layer remained in a forward onion state.[13] Figure 2(b) shows the resistance versus field measurements for configurations C1, C2, C3, and (C1-C3). Data from configurations C1 and C2 are plotted on the first *y* axis, and C3 on the second. The low resistance state corresponds to parallel magnetization in the NiFe and Co layers, while in the high resistance state the two layers are predominantly antiparallel. As expected, C1 and C2 have very similar resistances, while that of C3 is smaller by a factor of 2/3. This result supports the electrical model shown in Fig. 2(a). For all three configurations the GMR was 1.85%, calculated as $[(R_{max}\text{-}R_{sat})/R_{sat}] \times 100$, where R_{max} is the maximum resistance and R_{sat} is the resistance at saturation. All configurations show an increase in resistance of 0.70 Ω close to zero applied field [see Fig. 2(b)], but unlike C1 and C2, C3 also shows a dip in resistance at 20 Oe. The difference between the resistance data for C1 and C3, $[R(C1) - R(C3)]$ [see Fig. 2(b)], only shows a small step. The quantity $[R(C1) - R(C3)]$ is given by $R_A R_C/(R_1 + R_A + R_B + R_C)$, and this suggests that the step observed can be attributed to the initial propagation of reverse domains in sections R_A and R_C of the NiFe, as predicted by the simulation. This precedes the major resistance change seen in the measurements of C1, C2, and C3, which occurs close to zero applied field, and which is attributed to the reversal of the NiFe along the two sides of the ring.

In summary, ring-shaped magnetic structures are particularly interesting geometries for magnetotransport measurements because of the existence of two possible current paths. The measured magnetoresistance of the ring depends strongly on the contact geometry, as well as on the direction of the applied field. For NiFe elliptical rings the measured resistance and anisotropic magnetoresistance are quantitatively explained by micromagnetic and electrical modelings. The measured AMR depends on the positions of the domain walls with respect to the contacts, and shape anisotropy leads to different behaviors for fields applied along the major and minor axes. For a NiFe/Cu/Co pseudo spin valve elliptical ring, electrical measurements with different contact configurations allow the contributions of different sections of the ring to be identified, providing insight into the reversal process.

This work was supported by the Marie Curie Outgoing Fellowship Program, the Cambridge-MIT Institute, and the National Science Foundation. The authors gratefully acknowledge D. Bono and J. L. Prieto for fruitful suggestions and H. I. Smith for use of the nanofabrication facilities.

[1] J.-G. Zhu, Y. Zheng, and G. Prinz, J. Appl. Phys. **87**, 6668 (2000).
[2] M. Kläui, C. A. F. Vaz, L. Lopez-Diaz, and J. A. C. Bland, J. Phys.: Condens. Matter **15**, R985 (2003).
[3] F. J. Castaño, C. A. Ross, C. Frandsen, A. Eilez, D. Gil, H. I. Smith, M. Redjdal, and F. B. Humphrey, Phys. Rev. B **67**, 184425 (2003).
[4] M. Kläui, C. A. F. Vaz, J. A. C. Bland, W. Wernsdorfer, G. Faini, and E. Cambril, Appl. Phys. Lett. **81**, 108 (2002).
[5] M. Kläui, C. A. F. Vaz, J.A. C. Bland, W. Wernsdorfer, G. Faini, E. Cambril, L. J. Heyderman, F. Nolting, and U. Rüdiger, Phys. Rev. Lett. **94**, 106601 (2005); M. Kläui, C. A. F. Vaz, J. Rothman, J.A. C. Bland, W. Wernsdorfer, G. Faini, and E. Cambril, *ibid.* **90**, 097202 (2003).
[6] D. Buntinx, A. Volodin, and C. V. Haesendonck, Phys. Rev. B **70**, 224405 (2004).
[7] E. Saitoh, K. Harii, H. Miyajima, T. Yamaoka, and S. Okuma, Phys. Rev. B **71**, 172406 (2005).
[8] L. J. Heyderman, M. Kläui, B. Nöhammer, C. A. F. Vaz, J. A. C. Bland, and C. David, Microelectron. Eng. **73–74**, 780 (2004).
[9] M. M. Miller, G. A. Prinz, S. F. Cheng, and S. A. Bounnak, Appl. Phys. Lett. **81**, 2211 (2002).
[10] M.-F. Lai, Z.-H. Wei, C.-R. Chang, J. C. Wu, J. H. Kuo, and J.-Y. Lai, Phys. Rev. B **67**, 104419 (2003).
[11] J. Podbielski, F. Giesen, M. Berginski, N. Hoyer, and D. Grundler, Superlattices Microstruct. **37**, 341 (2005).
[12] F. J. Castaño, C. A. Ross, and A. Eilez, J. Phys. D **36**, 2031 (2003).
[13] F. J. Castaño, D. Morecroft, W. Jung, and C. A. Ross, Phys. Rev. Lett. **95**, 137201 (2005).
[14] OOMMF framework is available at http://math.nist.gov/oommf/